Supplemental Information

Brakemann et al.

Materials and Methods

Crystallographic analysis. The crystal structure of the non-fluorescent ground state of Padron0.9 (Padron0.9^{Off}) was solved by molecular replacement with Phaser (1) using the structure coordinates of non-fluorescent Dronpa (PDB 2POX) but omitting the chromophore. The partial structure was adjusted by manual model building with COOT (2) and refined with Refmac5 (3). After convergence, the chromophore was placed manually into vacant patches of the $2F_o$ - F_c and $F_o - F_c$ electron densities. The water structure was automatically built with Arp/wArp (4) and completed manually. For the fluorescent ground state structure (Padron0.9^{On}), structure solution and refinement were performed as outlined above, but for molecular replacement the structure coordinates of the Padron0.9^{Off} without chromophore were used.

Protein characterization. Prior to the determination of the absorption, excitation and fluorescence spectra, a 2 µl protein solution was quantitatively transferred into the off- or the on-state by irradiation with UV light (405 ± 5 nm) or blue light (488 ± 5 nm), respectively. A standard fluorescence microscope equipped with a 20× air objective lens (N Plan 0.40 NA) was used for the switching, which was monitored by measuring the fluorescence signal. After maximal switching, the proteins were diluted and the absorption and the emission spectra were immediately recorded with a Varian Cary 4000 UV/VIS spectrophotometer and a Varian Cary Eclipse fluorescence spectrophotometer (Varian, Palo Alto, CA, USA), respectively. For the emission spectra, rsFastLime, Padron0.9 and Dronpa were irradiated with 488 nm.

After switching the purified proteins into the on-state, the fluorescence quantum yields and the molar extinction coefficients at the respective absorption maximum were determined relative to the reported value of EGFP (quantum yield: 0.60, molar extinction coefficient at 489 nm: 56000 $M^{-1}\cdot cm^{-1}$) (5).

For the determination of the relaxation half-time from the on-state (Padron0.9, Padron-L141P) into the thermal equilibrium state, the proteins were expressed in *E. coli* and the cells were suspended in 1% low melting-point agarose. A 1.5 µl aliquot of this suspension was placed in a microtitre well, covered by a coverslip and sealed with Vaseline. After complete switching, the relaxation into the equilibrium state was followed at room temperature in the dark by consecutive short measurements with 5.6 $mW \cdot cm^{-2}$ blue light. The relaxation halftimes of rsFastLime and Dronpa were taken from (6).

Molecular dynamics simulations. Starting coordinates for the molecular dynamics based free energy calculations were taken from the x-ray structures of Padron0.9^{On} and Padron0.9^{Off}. Protonation states of titratable residues were chosen based on their reference pK_a values and structural criteria, such as hydrogen bond networks. For the simulations at high pH, we assumed all carboxylic acid groups to be deprotonated, as well as all cysteine side chains. All simulations were performed using the AMBER03 force field (7) and a periodic cubic box of approximately 7.5 x 7.5 x 7.5 nm^3. Crystal waters were retained. After adding about 13000 TIP3P water molecules (8), 4 potassium ions and 1 hydronium to neutralize the simulation system, both systems consisted of approximately 43000 atoms.

Equilibrium bond lengths, angles and torsions for the trans and cis chromophores were obtained by performing a geometry optimization on the isolated cis and trans chromophores at the B3LYP/6-31G* level of theory (9, 10) using Gaussian03 (11). The force constants for these interactions were taken from Reuter *et al*. (12). Chromophore partial charges for both the cis and trans configuration were obtained by fitting atomic charges to the electrostatic potential generated by the electron density as described in Ref. (13), computed at the B3LYP/6-31G* level.

Prior to the free energy calculations, both systems were equilibrated for 50 ns, with the root mean square deviation (RMSD) of the protein with respect to the X-ray structure levelling off at approximately 0.10 nm after 2 ns. The equilibrations were run at a constant pressure and temperature by coupling to an external bath (14), with time constants of 0.1 ps and 1.0 ps for the temperature and pressure coupling, respectively. The LINCS algorithm was used to constrain bond lengths (15), allowing a time step of 2 fs in the classical simulations. SETTLE was applied to constrain the internal degrees of freedom of the water molecules (16). A twin-range cut-off method

was used for non-bonded van der Waals interactions, which were modelled by the Lennard-Jones potentials: interactions within 1.0 nm were calculated at every timestep, whereas interactions between 1.0 and 1.6 nm were calculated every ten steps. Coulomb interactions were computed with the smooth Particle Mesh Ewald method (17), using a 1.0 nm real-space cut-off and a grid spacing of 0.12 nm. The relative tolerance at the real-space cut-off was set to 10^{-5}. All simulations were performed with the Gromacs-4.0 molecular dynamics program (18).

The change in free energy upon adding a proton to the anionic chromophore was determined by thermodynamic integration with a coupling parameter λ (19):

$$\Delta G = \int_0^1 d\lambda \left\langle \frac{\partial H(\lambda)}{\partial \lambda} \right\rangle_\lambda ,$$

where ΔG is the free energy difference between the deprotonated state ($\lambda = 0$) and the protonated state ($\lambda = 1$). The (classical) Hamiltonian H is interpolated between these two states:

$$H(\mathbf{q},\mathbf{p},\lambda) = \lambda \cdot H_{prot.}(\mathbf{q},\mathbf{p}) + (1-\lambda) \cdot H_{deprot.}(\mathbf{q},\mathbf{p}),$$

where, **p** and **q** are the positions and momenta of all atoms in the system.

Classical molecular dynamics trajectories of 500 ps each were generated at 21 equidistant points along this interval, and the ensemble average $\langle \partial H/\partial \lambda \rangle_\lambda$ was computed, using the final 300 ps of each simulation. The ensembles were generated with a stochastic dynamics integrator running at 300 K with a friction coefficient of 0.5 ps^{-1}. From each set of 21 simulations, the free energy difference was obtained by numerical integration of $\langle \partial H/\partial \lambda \rangle_\lambda$ over λ.

We note that the above free energy differences between protonated and deprotonated states only includes the electrostatic interaction of the proton with its environment, but neither the enthalpy, the covalent bond, nor electronic polarization effects of the chromophore. Accordingly, comparison of the calculated free energy differences will

differ from the experimental ones by these missing contributions. Assuming the offset to be similar both for the trans and cis state, however, allows one to calculate the change of proton affinity upon chromophore isomerization, using the thermodynamic cycle shown in Suppl. Fig.6*A*.

$$\Delta\Delta G^{\mathrm{MM}} = \Delta G^{\mathrm{MM}}_{trans} - \Delta G^{\mathrm{MM}}_{cis},$$

Because of the close contact between the O_2 oxygen atom of the five-membered ring and the six-membered ring, the trans configuration is less planar than the cis. As charge delocalization is strongly dependent on the degree of planarity in the chromophore, we have estimated this effect by calculating free energy differences between the force field level (MM) and the mixed quantum/classical (QM/MM) level using the thermodynamic cycle in Suppl. Fig.6*B*,

$$\Delta G^{\mathrm{QM}}_{trans} = \Delta G^{\mathrm{MM}}_{trans} + \Delta G^{\mathrm{MM\text{-}QM}}_{\mathrm{neutral}} - \Delta G^{\mathrm{MM\text{-}QM}}_{\mathrm{anion}},$$

and similarly for the cis configuration. From these values, the quantum mechanic correction for the change of proton affinity upon isomerization,

$$\Delta\Delta G^{\mathrm{QM}} = \Delta G^{\mathrm{QM}}_{trans} - \Delta G^{\mathrm{QM}}_{cis},$$

was obtained. The chromophore was described at the QM level. The remainder of the system was described with the Amber03 forcefield. The chemical bonds between C_1 and $C_{\alpha 1}$ and between N_3 and $C_{\alpha 3}$ that physically connect the QM and the MM subsystems were replaced by constraints, and the QM part was capped with two hydrogen link atoms. A mechanical embedding scheme was employed to describe the QM/MM interactions: interactions within the QM subsystem were described at the B3LYP/6-31G* level of theory, while both bonded and non-bonded interactions with the rest of the system were described at the Amber03 force field level.

The free energy difference ($\Delta G^{\mathrm{MM-QM}}$) between the force field Hamiltonian and the QM/MM Hamiltonian was computed using the force field ensemble (MM) via Boltzmann averaging (20),

$$\Delta G^{\mathrm{MM-QM}} = G_{\mathrm{QM}} - G_{\mathrm{MM}} = -k_B T \ln\left\langle \exp\left[-\left(V_{\mathrm{QM}}^{\mathrm{pot}} - V_{\mathrm{MM}}^{\mathrm{pot}}\right)/k_B T\right]\right\rangle_{\mathrm{MM}},$$

where k_B is the Boltzmann constant, T the temperature, and V^{pot} the total potential energy of the system evaluated with the MM and QM Hamiltonian, respectively. For the average, configurations at λ = 0 and λ = 1, respectively, were recorded at every picosecond during the above thermodynamic integration calculations that were used to compute ΔG^{MM}, and the potential energy $V_{\mathrm{QM}}^{\mathrm{pot}}$ was re-evaluated at the QM/MM level for all recorded configurations. All QM/MM potential energy computations were performed with the gromacs QM/MM interface (21) to the Gaussian program (11).

The combination of MM thermodynamic integration with QM/MM free energy perturbation was repeated ten times, starting from coordinates, taken at 1.0 ns intervals from a 10.0 ns equilibrium simulation for both the “on” and “off” state of Padron0.9. The final QM-corrected free energy of protonation in each state was computed as the average over these ten calculations. Independent error estimates were obtained from the standard deviations of these averages.

Supplemental References

1. McCoy AJ et al. (2007) Phaser crystallographic software. J Appl Crystallogr 40:658-674.
2. Emsley P, Cowtan K (2004) Coot: model-building tools for molecular graphics. Acta Crystallogr D Biol Crystallogr 60:2126-2132.
3. Murshudov GN, Vagin AA, Dodson EJ (1997) Refinement of macromolecular structures by the maximum-likelihood method. Acta Crystallogr D Biol Crystallogr 53:240-255.
4. Morris RJ, Perrakis A, Lamzin VS (2003) ARP/wARP and automatic interpretation of protein electron density maps. Methods Enzymol 374:229-244.
5. Patterson GH, Knobel SM, Sharif WD, Kain SR, Piston DW (1997) Use of the green fluorescent protein and its mutants in quantitative fluorescence microscopy. Biophys J 73:2782-2790.
6. Andresen M et al. (2008) Photoswitchable fluorescent proteins enable monochromatic multilabel imaging and dual color fluorescence nanoscopy. Nat Biotechnol 26:1035-1040.
7. Duan Y et al. (2003) A point-charge force field for molecular mechanics simulations of proteins based on condensed-phase quantum mechanical calculations. J Comput Chem 24:1999-2012.
8. Jorgensen WL, Chandrasekhar J, Madura JD, Impey RW, Klein ML (1983) Comparison of simple potential functions for simulating liquid water. J Chem Phys 79:926-935.
9. Becke AD (1993) A new mixing of Hartree-Fock and local density-functional theories. J Chem Phys 98:1372-1377.
10. Lee C, Yang W, Parr RG (1988) Dynamic behavior of endoplasmic reticulum in living cells. Phys Rev B Condens Matter 37:785-789.
11. Frisch MJ et al. (2004) Gaussian 03, Revision C.02 in *Gaussion, Inc., Wallingford, CT*.
12. Reuter NHL, Thiel W (2002) Green fluorescent proteins: Empirical force field for the neutral and deprotonated forms of the chromophore. Molecular dynamics simulations of the wild type and S65T mutant. J Phys Chem B 106:6310-6321.

13. Breneman CM, Wiberg KB (1990) Determining atom-centered monopoles from molecular electrostatic potential - the need for high sampling density in formamide conformational-analysis. J Computational Chemistry 11:361-373.
14. Berendsen HJC, Postma JPM, Van Gunsteren WF, Dinola A, Haak JR (1984) Molecular dynamics with coupling to an external bath. J Chem Phys 81:3684-3690.
15. Hess B, Bekker H, Berendsen HJC, Fraaije JGEM (1997) LINCS: A linear constraint solver for molecular simulations. J Computational Chemistry 18:1463-1472.
16. Miyamoto S, Kollman PA (1992) SETTLE - an analytical version of the shake and rattle algorithm for rigid water models. J Computational Chemistry 13:952-962.
17. Essmann U et al. (1995) A smooth particle mesh ewald method. J Chem Phys 103:8577-8593.
18. Hess B, Kutzner C, Van der Spoel D, Lindahl E (2008) GROMACS 4: Algorithms for Highly Efficient, Load-Balanced, and Scalable Molecular Simulation. J Chem Theory and Computation 4:435-447.
19. Kirkwood JG (1935) Statistical mechanics of fluid mixtures J Chem Phys 3:300-313.
20. Zwanzig RW (1954) High-temperature equation of state by a perturbation Method. I. Nonpolar gases. J Chem Phys 22:1420-1426.
21. Van der Spoel D et al. (2005) Gromacs, fast, flexible and free. J Computational Chemistry 26:1701-1718.
22. Davis IW et al. (2007) MolProbity: all-atom contacts and structure validation for proteins and nucleic acids. Nucleic Acids Res 35:W375-383.
23. Andresen M et al. (2007) Structural basis for reversible photoswitching in Dronpa. Proc Natl Acad Sci USA 104:13005-13009.
24. Stiel AC et al. (2007) 1.8 A bright-state structure of the reversibly switchable fluorescent protein Dronpa guides the generation of fast switching variants Biochem J 402:35-42.
25. Moors SLC et al. (2008) How is cis-trans isomerization controlled in Dronpa Mutants? A replica exchange molecular dynamics study. J Chem Theory and Computation 4:1012-1020.

26. Andresen M et al. (2005) Structure and mechanism of the reversible photoswitch of a fluorescent protein. Proc Natl Acad Sci USA 102:13070-13074.
27. Henderson JN, Ai HW, Campbell RE, Remington SJ (2007) Structural basis for reversible photobleaching of a green fluorescent protein homologue. Proc Natl Acad Sci USA 104:6672-6677.
28. Adam V et al. (2008) Structural characterization of IrisFP, an optical highlighter undergoing multiple photo-induced transformations. Proc Natl Acad Sci USA105:18343-18348.
29. Wallace AC, Laskowski RA, Thornton JM (1995) LIGPLOT: a program to generate schematic diagrams of protein-ligand interactions. Protein Eng 8:127-134.

Supplemental Tables and Figures

Fluorescent protein	Absorption max on-/off-state (nm)	Emission max. (nm)	Ext. coeff. (M^{-1}•cm^{-1})	Fluorescence quantum yield	Off-state fluorescence	Relaxation half-time	Equilibrium (% fluor. max.)
Padron0.9	504 (395) / 504	524	36 000	0.61	0.4%	250 min	7%
Padron0.9-L141P	502 (396) / 492 (395)	519	49 000	0.58	2.9%	700 min	11%
Padron	503 (396) /505	522	43 000	0.64	0.7%	150 min	5%
Dronpa	503 / 392	522	115 000	0.68	6.0%	840 min	100%

Supplemental Table 1: Detailed properties of the fluorescent proteins analyzed in this study. Secondary absorption maxima are written in parentheses.

Data Collection		
	Padron0.9-Off	**Padron0.9-On**
Wavelength (Å)	1.0000	1.0000
Temperature (K)	100	100
Space Group	$P2_12_12_1$	$P2_12_12_1$
Unit Cell Parameters (Å)	73.33 104.26 123.10	72.86 103.81 121.21
Resolution (Å)	50-1.80 (1.86-1.80)[a]	50-1.65 (1.71-1.65)
Reflections		
Unique	88654	109915
Completeness (%)	99.7 (99.4)	99.7 (100)
Redundancy	5.9 (5.6)	3.6 (3.6)
I/σ(I)	24.7 (2.3)	18.4 (1.4)
R_{sym}(I)[b]	0.045 (0.557)	0.036 (0.618)
Refinement		
Resolution (Å)	30-1.80	20-1.65
Reflections		
Number	88388	109667
Completeness (%)	99.2	99.3
Test Set (%)	5.1	4.7
R_{work}[c]	15.9	16.8
R_{free}[c]	27.0	20.0
R_{all}[c]	16.1	16.9
ESU (Å)[d]	0.071	0.069
Contents of A.U.[f]		
Protein Molecules/Residues/Atoms	4/875/7642	4/878/7451
Water Oxygens	744	680
Ligand Molecules/Atoms	10/103	11/94
Ramachandran Plot[g]		
Favored	99.88	99.42
Allowed	0.12	0.58
Outliers	-	-
Rmsd[h] **from Target Geometry**		
Bond Lengths (Å)	0.011	0.013
Bond Angles (°)	1.33	1.45
Rmsd B-Factors (Å^2)		
Main Chain Bonds	0.574	0.783
Main Chain Angles	1.141	1.471
Side Chain Bonds	2.042	2.514
Side Chain Angles	3.246	4.041
PDB ID	3LSA	3LS3

[a] Data for the highest resolution shell in parentheses

[b] $R_{sym}(I) = \Sigma_{hkl}\Sigma_i |I_i(hkl) - \langle I(hkl)\rangle| / \Sigma_{hkl}\Sigma_i |I_i(hkl)|$; for n independent reflections and i observations of a given reflection; $\langle I(hkl)\rangle$ – average intensity of the i observations

[c] $R = \Sigma_{hkl} ||F_{obs}| - |F_{calc}|| / \Sigma_{hkl} |F_{obs}|$; R_{work} – $hkl \notin T$; R_{free} – $hkl \in T$; R_{all} – all reflections; T – test set

[d] ESU – estimated overall coordinate error based on maximum likelihood

[f] A.U. – asymmetric unit

[g] Calculated with MolProbity (http://molprobity.biochem.duke.edu/) (22)

[h] Rmsd – root-mean-square deviation

Supplemental Table 2: Crystallographic Data and Refinement

	cis chromophore (on)		trans chromophore (off)	
t_{start} (ns)	ΔG (kJ/mol) Amber03	ΔG (kJ/mol) B3LYP/6-31G*	ΔG (kJ/mol) Amber03	ΔG (kJ/mol) B3LYP/6-31G*
2.0	137.7 ± 1.3	-1105.3 ± 1.3	141.6 ± 0.6	-1097.0 ± 0.6
3.0	136.2 ± 1.5	-1109.4 ± 1.5	150.9 ± 0.9	-1089.1 ± 0.9
4.0	141.0 ± 3.3	-1101.2 ± 3.3	151.9 ± 1.0	-1085.7 ± 1.0
5.0	138.2 ± 3.7	-1111.0 ± 3.7	143.4 ± 1.4	-1095.3 ± 1.4
6.0	134.3 ± 2.5	-1106.8 ± 2.5	141.9 ± 0.7	-1097.0 ± 0.7
7.0	139.8 ± 3.2	-1102.3 ± 3.2	146.0 ± 1.0	-1098.1 ± 1.0
8.0	131.7 ± 3.3	-1109.7 ± 3.3	146.8 ± 1.0	-1095.9 ± 1.0
9.0	140.2 ± 1.6	-1099.6 ± 1.6	135.4 ± 1.5	-1097.6 ± 1.5
10.0	137.6 ± 2.9	-1106.8 ± 2.9	142.8 ± 1.2	-1095.4 ± 1.2
11.0	137.5 ± 0.9	-1106.1 ± 0.9	140.6 ± 1.0	-1094.2 ± 1.0
⟨ΔG⟩	137.4 ± 2.6	-1105.8 ± 2.6	144.1 ± 1.3	-1094.5 ± 1.3

Supplemental Table 3: Computed free energies for protonating the chromophore. Values were derived from snapshots taken in 1 ns intervals from a 11 ns Padron0.9 simulation. Both the free energies computed at the forcefield level and at the QM/MM corrected B3LYP/6-31G* level are listed for the On and Off states of Padron. Since at 300 K one pK_a unit equals 5.74 kJmol^{-1} ($RT\ln[10]$), the $\Delta\Delta G$ of 11.3 ± 2.1 corresponds to a drop in pK_a of 2.0 ± 0.4 units.

	$\langle\Delta G\rangle_{on}$	$\langle\Delta G\rangle_{off}$	$\langle\Delta\Delta G\rangle$	ΔpK_a
A	-1105.8 ± 2.6	-1094.4 ± 1.3	11.4 ± 2.1	-2.0 ± 0.4
B	-1122.4 ± 2.2	-1122.7 ± 2.0	-0.3 ± 2.1	0.1 ± 0.4
C	-1083.6 ± 1.4	-1093.7 ± 2.2	-10.1 ± 1.8	1.8 ± 0.3
D	-1080.9 ± 1.5	-1093.5 ± 3.2	-12.6 ± 2.5	2.2 ± 0.4

Supplemental Table 4: **Calculated average free energies in kJmol^{-1} for protonating the chromophore in different active site configurations.** $\langle\Delta\Delta G\rangle$ is the average calculated difference in protonation free energies between the On (cis) and Off (trans) states. The last column lists the resulting shift in pK_a upon conversion from the cis to the trans configuration in Padron0.9.

		Θ	Tilt (τ)	Twist (φ)	Modulus of sum*	Sum of moduli**
Padron0.9 [a]	**cis**	22.3 ± 0.8	16.1 ±1.8	-27.7 ± 1.8	11.6 ± 1.1	43.8 ± 3.4
	trans	22.7 ± 1.4	-20.7 ± 1.3	-2.31 ± 3.3	22.3 ± 2.1	23.5 ± 1.0
Dronpa [a] (23, 24)	**cis**	13.0 ± 2.1	12.2 ± 1.7	-15.9 ± 2.5	3.7 ± 1.4	28.1 ± 4.9
	trans	26.6 ± 4.7	-19.5 ± 4.5	40.1 ± 6.3	20.6 ± 5.3	59.6 ± 9.5
Dronpa [b] (neutral) (25)	**cis**	10.0 ± 5.5	0.3 ± 6.1	-7.1 ± 5.9	6.8	7.4
	trans	17.9 ± 8.7	1.1 ± 6.8	-10.0 ± 7.4	8.9	11.1
rsFastLime [b] (neutral) (25)	**cis**	19.8 ± 10.5	0.4 ± 6.6	-16.2 ± 13.0	15.8	16.6
	trans	35.8 ± 8.5	-8.3 ± 6.8	-25.8 ± 11.1	34.1	34.1
rsFastLime [b] (anion) (25)	**cis**	11.6 ± 6.2	3.0 ± 7.0	-4.6 ± 9.2	1.6	7.6
	trans	-	-	-	-	-
asFP-A143S [a] (26)	**cis**	24.1 ± 5.0	36.8 ± 8.0	-26.5 ± 9.5	10.3 ± 1.5	63.3 ± 17.5
	trans	24.1 ± 1.6	-20.0 ± 0.8	34.6 ± 1.4	14.7 ± 2.3	54.5 ± 0.6
mTFP0.7 [a] (27)	**cis**	13.1 ± 1.0	14.6 ± 0.8	-16.0 ± 0.4	1.5 ± 0.8	30.6 ± 2.4
	trans	56.4 ± 0.7	-16.7 ± 1.3	66.8 ± 0.4	50.1 ± 1.7	83.5 ± 0.9
IrisFP [a] (green state) (28)	**cis**	13.6 ± 0.6	5.7 ± 1.7	-18.1 ± 1.1	12.4 ± 0.7	23.8 ± 2.7
	trans	40.2 ± 7.0	-3.5 ± 0.7	43.8 ± 6.6	40.2 ± 6.8	47.3 ± 6.4

[a]: X-ray structure
[b]: calculated structure
*: modulus of the sum of τ and φ
**: sum of the moduli of τ and φ

Supplemental Table 5: Torsion of the chromophores of various photochromic proteins in the fluorescent (cis) and the non-fluorescent state (trans). Given angles are mean values with standard deviations with respect to the available protomers. θ denotes the angle between the planes spanned by the two chromophoric rings. The modulus of the sum of τ and φ describes the torsion of the chromophore.

	$\langle \Delta G_{prot} \rangle$, pH ≈ 7	$\langle \Delta G_{prot} \rangle$, pH ≈ 10	$\langle \Delta\Delta G_{prot} \rangle$	ΔpK_a
Padron0.9	137.4 ± 2.6	112.6 ± 2.5	-24.8 ± 2.6	+4.4± 0.4
Padron0.9-C62S	117.4 ± 1.6	91.3 ± 1.5	-26.1 ± 1.6	+4.6 ± 0.3
Padron0.9-C62S,C171S	125.3 ± 3.5	99.3 ± 1.7	-26.0± 1.9	+4.5 ± 0.3
Padron0.9-C171S	142.4 ± 1.0	118.7 ± 1.9	-23.7 ± 1.5	+4.1 ± 1.6

Supplemental Table 6: Protonation free energies (without QM/MM correction) for the cis conformation of the chromophore at normal pH (approx. 7.0) and high pH (approx. 10.0) for Padron0.9 and the indicated variants.

Supplemental Figure 1: Amino acid alignment of the proteins Dronpa, Padron and Padron0.9.

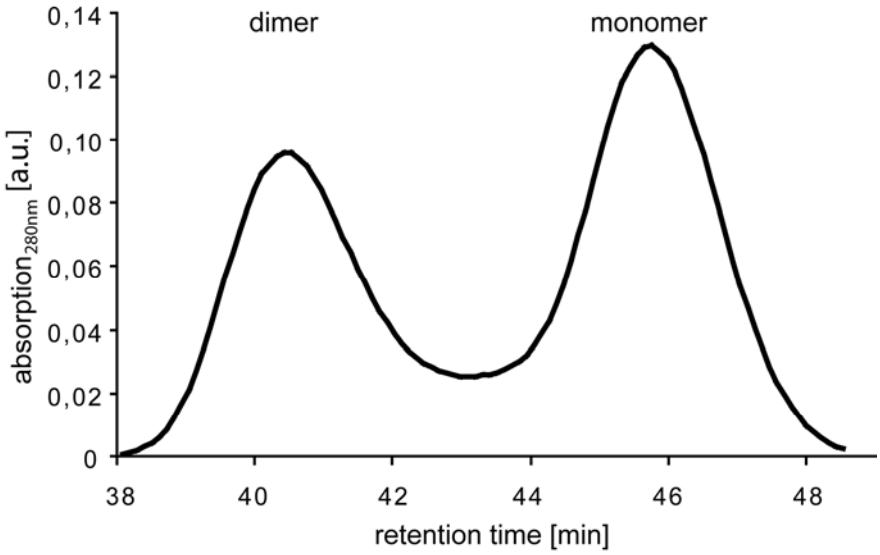

Supplemental Figure 2: Size separation chromatography of Padron0.9. Purified protein was taken up in 100 mM Tris HCl, 150 mM NaCl, pH 7.5 at a concentration of ~10 mg·ml^{-1} and separated on a SMART FPLC system (GE Healthcare, Uppsala, Sweden) using a Superdex 200 PC 3.2/30 column at room temperature. The protein was stored at 4°C before injection.

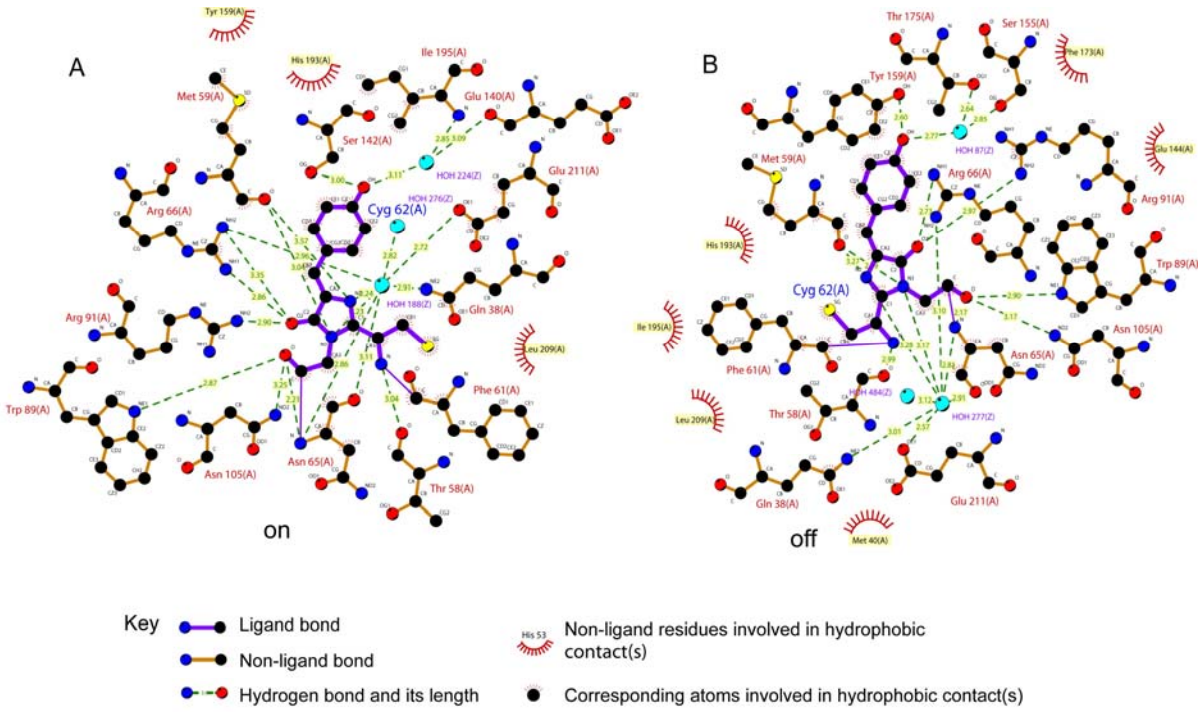

chain	A	B	C	D
		Padron0.9-ON		
H-bonds	8	8	8	8
water-mediated H-bonds	3	2	4	2
		Padron0.9-OFF		
H-bonds	9	9	8	8
water-mediated H-bonds	3	3	3	3

Supplemental Figure 3: Ligplot representations of the chromophores in Padron0.9^{On} (A) and Padron0.9^{Off} (B). The depicted ligplots were calculated in both cases on the protomer A with the program LIGPLOT (29). The table shows the number of H-bonds for each of the protomers in the structures. Both chromophores are attached to a similar extend to the protein matrix.

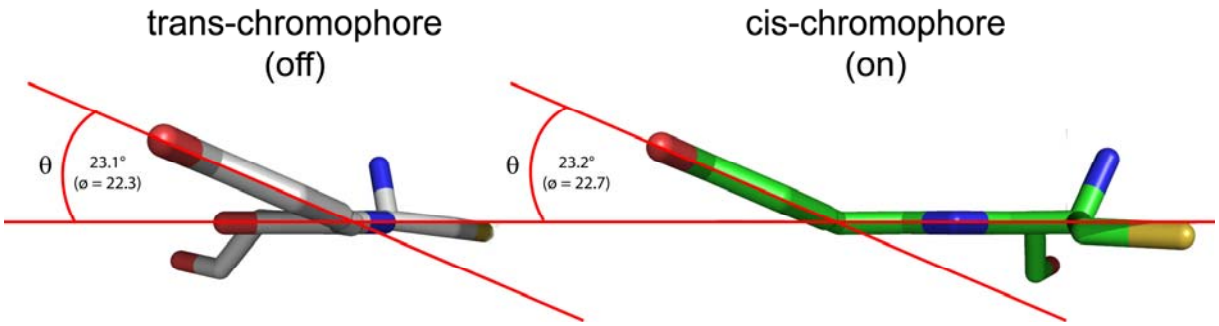

Supplemental Figure 4: Angles θ between the planes spanned by the imidazolinone- and the tyrosyl-ring. Depicted are the protomer A of Padron0.9^{On} (cis-chromophore) and Padron0.9^{Off} (trans-chromophore). The average values (over all four protomers) for θ are given in parenthesis. θ is highly similar in the fluorescent and the non-fluorescent states of Padron0.9.

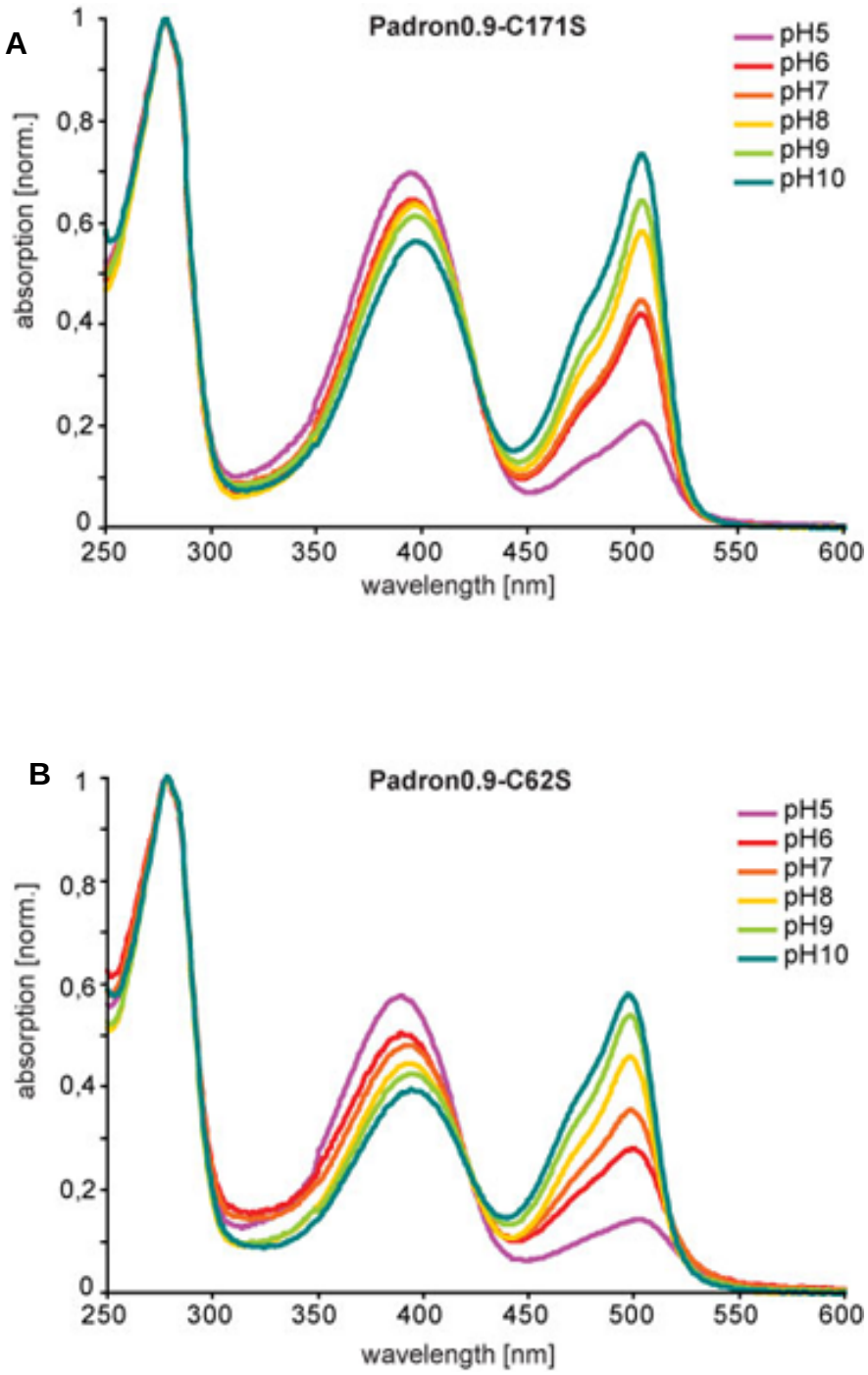

Supplemental Figure 5: pH dependence of the On-state absorption spectra of Padron0.9-Cys171Ser and Padron0.9-Cys62Ser.

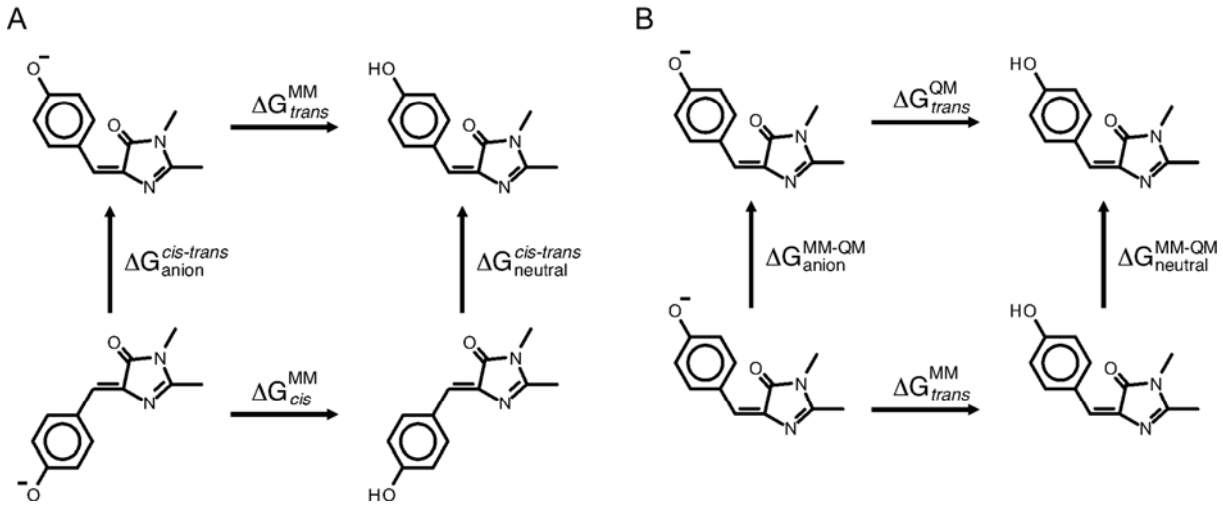

Supplemental Figure 6: Scheme of thermodynamic states of the Padron0.9 chromophore. (A) Thermodynamic cycle used in the simulations to compute the difference between $\Delta G_{trans}^{\mathrm{MM}}$ and $\Delta G_{cis}^{\mathrm{MM}}$. (B) Thermodynamic cycle used to compute the free energy required to transform the classical ensemble into a mixed quantum/classical (QM/MM) ensemble.